RESEARCH

Multi-transcriptomics reveals niche-specific expression programs and endothelial cells in glioblastoma

Jiukun Hu[1,2†], Xiaohan Sa[1,2†], Yue Yang[2,3], Yuwen Han[1,2], Jie Wu[4], Minxuan Sun[1,2], Shaheryar Shafi[1,2], Nafees Ahmad[5], Sami Siraj[6], Jiao Yang[7]* and Yuanshuai Zhou[1,2]*

Abstract

Background Glioblastoma (GBM) is a highly lethal malignant intracranial tumor, distinguished from low-grade glioma by histopathological hallmarks such as pseudopalisading cells around necrosis (PAN) and microvascular proliferation (MVP). To date the spatial organization of the molecular and cellular components of these specific histopathological features has not been fully elucidated.

Methods Here, using bulk RNA sequencing, spatial transcriptomic and single cell RNA sequencing (scRNA-seq) data of GBM patients, we identified niche-specific transcriptional programs and characterized the differences in molecular expression and cellular organization between PAN and MVP.

Results Notably, we discovered spatially distinct domains within the tumor core and identified niche-specific signatures: NDRG1 and EPAS1, specifically expressed in the PAN and MVP regions. The clustering results showed two distinct phenotypes of endothelial cells (ECs) were enriched in the MVP and PAN regions, respectively. PAN-associated endothelial cells exhibit copy number variations similar to those in GBM cells. Single cell trajectory analysis reveals a pseudotime trajectory, indicating the differentiation of glioblastoma stem cells (GSCs) toward ECs.

Conclusions Necrosis cores which are surrounded by hypoxic and perivascular niches and microvascular proliferation area within the glioblastoma tumor microenvironment, have been considered as standardized morphological indicators of aggressive GBM. Our findings provide a cellular and molecular insights into GBM progression.

Keywords Glioblastoma, Spatial transcriptomes, Pseudopalisading cells around necrosis, Microvascular proliferation, Endothelial cells

†Jiukun Hu and Xiaohan Sa contributed equally to this work.

*Correspondence:
Jiao Yang
yangjiaomed@126.com
Yuanshuai Zhou
zhouys@sibet.ac.cn

Full list of author information is available at the end of the article

Introduction

Glioblastoma (GBM) is a highly malignant, rapidly progressive brain tumor that is pathologically characterized by pseudopalisading cells around necrosis (PAN) and microvascular proliferation (MVP) [1, 2]. These histological features distinguish GBM from lower-grade brain tumors and have long been recognized as ominous prognostic features.

PAN refers to a hypercellular zone surrounding necrotic areas in GBM, while MVP is a form of angiogenesis morphologically recognized as endothelial proliferation within newly sprouted vessels. PAN and MVP have been considered as indicators of the high malignancy and invasive capacity of GBM. However, the pathogenesis of this organizational structure remains unclear. One generally accepted theory is that GBM cells overgrowth leads to intratumorally vascular damage, resulting in endothelial injury that exacerbates tissue hypoxia. Malignant cells migrate away from the hypoxic environment, forming waves that move toward the periphery and appear as pseudoapoptotic cells under the microscope. Additionally, tumor cells in the hypoxic area secrete vascular endothelial growth factor (VEGF) and IL-8, promoting microvascular proliferation and accelerating the outward expansion of tumor cells alongside new blood vessel formation. Despite considerable advances in molecular mechanisms involved in GBM tumorigenesis in recent decades, the molecular and cellular heterogeneity of these hallmark regions and their spatial characteristics have not been fully elucidated [3, 4].

GBM contains a host of non-tumor components like mesenchymal cells, vasculature, cytokines, immune cells, and fibroblasts, constituting a complex tumor microenvironment (TME) with many anatomically distinct regions. Necrosis cores which are surrounded by hypoxic and perivascular niches within the GBM TME, have been considered as a standardized morphological indicator of aggressive GBM. However, the pathogenesis of these regions in malignant GBM is not fully understood. Therefore, clarifying the molecular characteristics of specific regions and targeting therapies based on these signatures may prove a promising treatment strategy. The Ivy Glioblastoma Atlas Project (Ivy GAP) has collected genomic and transcriptomic profiles of anatomical regions like PAN, MVP and cellular tumor (CT). Accordingly, the database can enable understanding of molecular diversity relating to histological heterogeneity. Nevertheless, few studies revealed the spatial heterogeneity of molecular signatures in diverse cellular states from PAN and MVP. The development of spatially resolved transcriptomics (SRT) technology enables us to elaborate the correlation between characteristic gene expression profiles while retaining information of the spatial tissue context and histological structures within tumors.

Here, we integrate RNA sequencing, SRT, and single-cell RNA sequencing (scRNA-seq) to characterize differences between GBM structures, uncovering cellular heterogeneity and molecular stratification of histologic structures within GBMs. We identified prognostic and predictive markers corresponding to GBM localizations.

Methods

Description of the datasets

The RNA-seq datasets ($n = 41$) from different anatomical regions of primary human glioblastoma (GBM) were obtained from the Ivy Glioblastoma Atlas Project (Ivy-GAP). Additionally, spatially resolved transcriptomics (SRT) datasets ($n = 16$) of human GBM samples lacking IDH mutation, generated using Visium technology (10X Genomics), were sourced from Ravi et al. (https://doi.org/10.5061/dryad.h70rxwdmj). The Smart-seq2 glioblastoma scRNA-seq dataset ($n = 28$, GSE131928) was acquired from the GEO database. Lastly, the Cancer Genome Atlas (TCGA) GBM dataset ($n = 155$), containing RNA-sequencing and clinical data, was retrieved from the UCSC Xena browser (https://xenabrowser.net/).

Histological structure based differential gene expression analysis

Gene expression profiles from the CT, PAN, and MVP regions were extracted from the Ivy-GAP datasets. To normalize the gene expression values in Fragments Per Kilobase Million (FPKM) format, we applied a $\log2(n + 1)$ transformation of counts using the dplyr package (R 1.0.10). Data quality control and pairwise differential expression analysis among the three groups were conducted using the limma package (R 3.54.0) with a logFoldChange cutoff of 1. Based on the differentially expressed genes (DEGs) identified between pairs, intersection queries were performed using the UPsetR package (R 1.4.0) to visualize shared and unique DEGs. Gene IDs were then converted from SYMBOL to ENTREZID format using the clusterProfiler package (R 4.6.0), and we conducted Gene Ontology (GO) enrichment analysis in the Biological Process (BP), Molecular Function (MF), and Cellular Component (CC) categories. Additionally, KEGG (Kyoto Encyclopedia of Genes and Genomes) pathway enrichment analysis was performed to further interpret the functional roles of DEGs across these regions.

Spatial transcriptomics analysis

For the analysis of spatially resolved transcriptomics, we followed the standard protocol recommended by Seurat (R 4.0). To ensure reproducibility, data from 16 libraries were merged and filtered using consistent criteria: cells with gene counts between 500 and 8000, total transcript counts below 30,000, and a mitochondrial gene

percentage below 30%. We applied the SCTransform function to normalize gene expression uniformly across all locations, maintaining default settings for consistency. Additionally, we used both Seurat and the SpaGCN toolkit (https://github.com/jianhuupenn/SpaGCN) to identify spatial variable genes (SVGs), with default parameters applied throughout. This dual approach allowed for cross-validation of SVG identification, enhancing reproducibility by verifying gene expression patterns across spatial domains. These combined methods facilitated the accurate characterization of tissue heterogeneity while ensuring methodological consistency.

Deconvolution

Bhaduri et al. [5] GBM scRNA-seq and Neftel et al. [6] SmartSeq2-derived human GBM scRNA-seq datasets were used as reference datasets. The "harmony" method was used to integrate the dataset from different specimens. The integrated reference is consisting of 40,791 cells, 22,346 genes and 20 cell types. The celltypes with < 1000 cells were filtered. we used the merged datasets as input for the subsequent deconvolution analysis. We used RCTD (v1.1.0, https://github.com/dmcable/space xr) to deconvolute the transcriptome of each spot (run. RCTD function with the entire mode parameter) into the likely constituent cell types. Deconvoluted ratios of individual cell types were visualized by Stdeconvolve and ggplot2 packages.

Single cell RNA-sequencing data analysis

The scRNA-seq datasets contains 6863 GBM cells and 1067 normal cells from 28 patients. Count tables were analyzed used Seurat 4.0 package following the standard workflow with default settings. Next, InferCNV package (R 1.3.3) was applied to infer CNV from scRNA-seq data, with cutoff = 1. We then combined the CNV classification with the UMAP-based and the gene-set based classifications to define the GSCs and GBM associated macrophage/macroglia. The marker genes for macrophages, T cells, and oligodendrocytes were obtained from Neftel et al. (GSE131928) [9]. To investigate the molecular interaction networks among each cell subtype, CellPhoneDB (R 2.1.7) algorithm was used to infer intercellular communication in the GSC niche.

Immunofluorescence

Clinical glioma paraffin slides were obtained from Wuhan Union Hospital. All samples were collected with signed informed consent according to the internal review and ethics boards of Wuhan Union Hospital. The procedure was approved by the ethics boards of Wuhan Union Hospital. After de-waxing and rehydrating, slides were boiled in Tris-EDTA antigen retrieval buffer (PH = 8.0) for 10 min. Next, sections were treated with 3% H_2O_2 for 10 min to bleach endogenous peroxidase. After blocking with donkey serum in PBS for 30 min, slides were incubated at 4 °C overnight with primary antibodies. Glioma slides were probed with primary antibodies against the following proteins: CD44 (eBioscience, San Diego, USA), and HIF2A/EPAS1 (Signalway Antibody, Greenbelt, USA), IGFBP7, THY1, NDRG1 and CD31 (Cell Signaling Technology, MA, USA). Sides were then washed with PBS and incubated with DyLight 488/ FluorTM Plus 647 conjugated donkey anti-rabbit, mouse or rat secondary antibody (Invitrogen) for 2 h away from light at room temperature and followed by DAPI staining for another 10 min. After washing away from light, the slides were sealed with an anti-fluorescence quenching sealer and the fluorescence was observed using an Olympus VS200 Slide Scanner.

RNA isolation and qPCR

Total RNA was extracted from HUVEC cell samples subjected to PAN and MVP region environment simulation using the RNAiso Plus reagent (TAKARA, 9109) according to the manufacturer's instructions. The extracted RNA was dissolved in RNase-free water, and its concentration and purity were determined using a Nano-Drop 2000 spectrophotometer (Thermo Fisher Scientific, USA), ensuring an A260/A280 ratio of 1.8–2.0. Subsequently, the RNA was reverse-transcribed into cDNA using the HiScript III RT SuperMix (Vazyme, R323-01) following the kit protocol. Quantitative real-time PCR was performed using the Taq Pro Universal SYBR qPCR Master Mix (Vazyme, Q712-02) on a real-time PCR instrument. All experiments were performed with three biological replicates and three technical replicates. qPCR data were analyzed using the ΔΔCt method to calculate the relative expression levels of target genes normalized to the GAPDH gene.

Results

Anatomical transcriptome analysis of glioblastoma revealed the molecular differences between PAN and MVP

To dissect heterogeneity within MVP and PAN anatomical structures hidden in bulk analysis and explore the distinct molecular signatures associated with GBM malignancy, we performed integrative bioinformatics analysis. This analysis incorporated histological structure-specific transcriptional profiles, spatial transcriptome datasets and single-cell transcriptome datasets (as illustrated in Fig. 1A).

In the Ivy-GAP dataset, we compared the profiles of 270 laser-microdissected GBM tissues, including samples from 111 cortical (CT), 22 hyperplastic blood vessels (HBV), 40 PAN, 28 MVP, 26 perinecrotic zone (PNZ), 24 infiltrating tumor (IT), and 19 leading edge (LE) regions (Fig. 1B). We compared expression profiles

Hu *et al. Journal of Translational Medicine*   (2025) 23:444

Page 4 of 13

between perivascular regions (HBV and MVP) and CT, as well as between perinecrotic regions (PNZ and PAN) and CT, using criteria of > 2-fold change and FDR < 0.05. PAN and PNZ showed similar expression profiles, as did HBV and MVP, reflecting their histologic similarities. Notably, PAN and PNZ had elevated expression of angiogenesis-promoting genes, including IL-8, ADM, VEGFA, and NDRG1, compared to other regions. HBV and MVP exhibited high expression of endothelial and stemness-associated genes such as ESM1 and CRIP1 [7, 8]. Additionally, MVP exhibited increased expression of tumorigenesis and migration-related molecules like HIGD1B and MMP9. Differentially expressed genes were more pronounced in PAN and MVP compared to PNZ and HBV. A Venn diagram of DEGs highlighted 312 genes specifically up-regulated in PAN and 1048 in MVP (Fig. S1A).

Interestingly, 151 down-regulated genes overlapped between PAN and MVP, comprising one-third of PAN downregulation. These were involved in nervous system development and cell adhesion (Fig. S1B and S1C). Gene Ontology and KEGG analysis of MVP DEGs showed association with ameboidal migration and pathways like PI3K-Akt and focal adhesion (Fig. S1D). PAN DEGs were enriched in hypoxia response and HIF-1 signaling (Fig. S1E). This suggests cells in PAN and MVP are highly malignant, with reduced intercellular adhesion facilitating invasion and aggressiveness.

Identification of domain-specific marker genes of PAN and MVP

To further characterize the spatial organization of morphologically distinct regions within GBM tumors, we employed the Seurat and SpaGCN packages to identify robust spatially variable genes (SVGs) in 10X Visium datasets. We integrated spots from the same cluster in each sample into pseudobulks using Seurat (Fig. S2).

To reveal the spatial distribution of upregulated genes, SRT datasets from 16 GBM patients were integrated, identifying 1000 and 524 SVGs through Seurat and SpaGCN, respectively (Table S1). Overlapping with PAN and MVP upregulated genes yielded 63 PAN and 53 MVP signature gene candidates (Fig. 1C and D). These were ranked by frequency in patient SVGs. The top PAN genes were IGFBP5, MTIX, CHI3L1, NDRG1, and VEGF. Top MVP genes were IGFBP, SPARC, IFITM3, IGFBP3 and A2M (Fig. 1E and F). Most of these associate with migration, invasion, stemness [9–11] and angiogenesis [12–14], which is consistent with the histological features and functions of PAN and MVP.

TCGA RNA seq data showed most signature genes had higher expression in GBM versus LGG (Fig. S3). Furthermore, high expression associated with poor prognosis (Fig. S4), including IGFBP5, IGFBP3, IGFBP7 and CHI3L1. This suggests PAN and MVP spatial upregulation of these genes may promote GBM malignancy.

The spatial localization of PAN and MVP signature genes

To clarify whether the PAN and MVP signature genes have specific spatial expression patterns, we compared their spatial expression in GBM patients. We selected UFK243 as a typical sample with obvious necrosis and vascular proliferation (Fig. 2A). UFK243 spots were clustered into 6 domains by Seurat and SpaGCN. We observed elevated APOC1 and NDRG1 in domain 0, EPAS1 and VEGFA in domain 1, and IGFBP7, CHI3L1 and TAGLN in domain 5 (Fig. 2B). PAN genes like IGFBP5, MT1X, CHI3L1 and NDRG1 had similar spatial patterns, predominantly in domains 0 and 5. Meanwhile, IGFBP7, IFITM3, A2M and EPAS1 were sporadic in domains 1, 3 and 5 (Fig. 2C). PAN and MVP genes also showed distinct spatial patterns in UFK243 (Fig. S5).

In situ hybridization from the Ivy GAP further verified elevated NDRG1 and EPAS1 in PAN (Fig. 3A). Immunofluorescence also validated the differences, showing high levels of NDRG1 and HIF2A in PAN (Fig. 3B). Consistently, immunofluorescence (IF) results from two additional clinical patient samples showed that IGFBP7 and THY1 were enriched around CD31-positive blood vessels (Fig. S6). These results confirm the accuracy of the obtained region-specific signature genes.

Identification of cell type composition in spatially resolved transcriptomic GBMs

The intricate glioma microenvironment consists of non-neoplastic cell types including endothelial cells, pericytes, microglia, macrophages, and fibroblasts. To comprehensively characterize these, integrated data was visualized by UMAP dimension reduction and unsupervised clustering (Fig. 4A and B). Using SingleR annotation and manual curation, we identified 9 major cell types: astrocytes, macrophage/microglia, neurons, oligodendrocytes, OPCs, fibroblasts, endothelial cells (ECs), T cells, and adipocytes (Fig. 4C). Additionally, spatial deconvolution was performed (Fig. S7). Notably, these methods were consistent, and paired SRT/scRNA analysis showed the identified proportions were comparable to scRNA (Fig. S8).

We examined the gene expression of 63 PAN and 53 MVP signature genes across cell types (Fig. 4D). Differences were most prominent in fibroblasts and endothelial cells. MVP genes showed elevated expression in fibroblasts and some endothelial cells, like COL4A1, COL4A2, and FN1. Meanwhile, PAN genes were highly expressed in most other endothelial cells, with CHI3L1 and NAMPT highest in endothelial cells followed by macrophage/microglia. The distinct endothelial expression
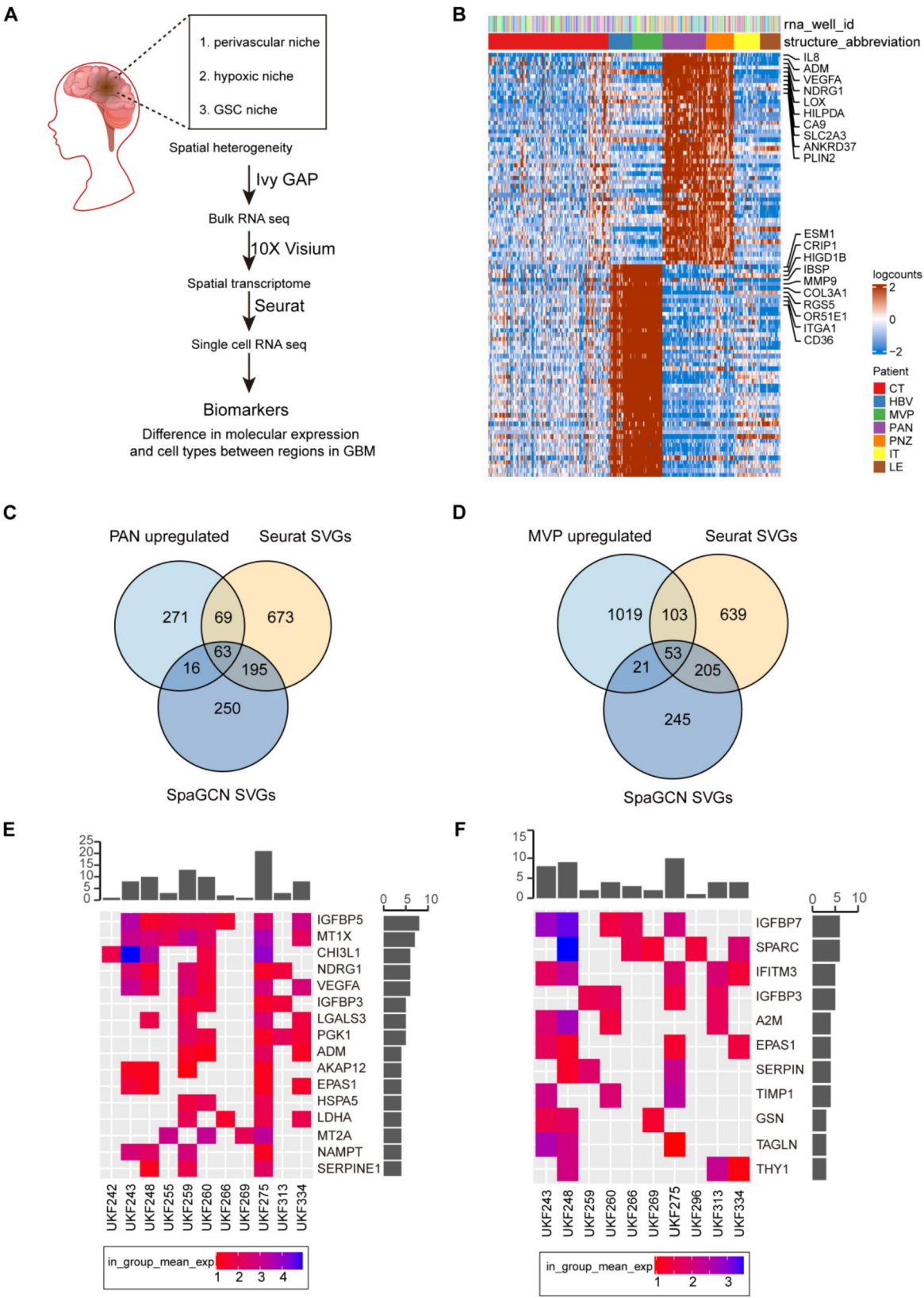
Fig. 1 (See legend on next page.)

Hu *et al. Journal of Translational Medicine*   (2025) 23:444

Page 6 of 13

(See figure on previous page.)

Fig. 1 Characterizing intra-tumoral expression heterogeneity in GBM by distinct molecular profiles. **A** Schematic representation of processing and integration of multi-level RNA sequencing data. RNA-seq datasets ($n=41$), Spatially resolved transcriptomics datasets (SRT, $n=28$) scRNA-seq dataset ($n=28$, GSE131928). **B** A heatmap of differentially expressed genes (rows) in distinct anatomical regions (columns). Expression differences in perivascular areas (including hyperplastic blood vessels [HBV], and areas of microvascular proliferation [MVP]) with cellular tumor (CT) and perinecrotic areas (perinecrotic zones [PNZ], pseudopalisading cells around necrosis [PAN]) with CT were compared in pairs (> 2 fold change, FDR < 0.05). IT, infiltrating tumor; LE, leading edge. **C, D** Venn diagrams representing the overlap between significantly up-regulated genes in Ivy GAP data, Seurat and SpaGCN spatially variable genes (SVGs) for PAN and MVP. **E, F** Expression of PAN and MVP associated signature genes in GBM patients. Genes with domain numbers greater than 3 points were listed. The bars at the top of the tile graph indicate the number of spatially variable expressed signature genes in each patient, and the bars on the right indicate the number of patients with spatially variable expression of each gene. The color indicates the level of expression

patterns suggest these cells may play different roles in PAN and MVP histological features.

Exploring diverse endothelial cells in human glioblastoma

PAN and MVP signature module scores also showed relatively independent distribution (Fig. 5A and B), suggest that endothelial cells in these regions have distinct expression patterns and functional states. To understand endothelial heterogeneity, unsupervised clustering was performed (Fig. 5C and D). Differential expression analysis revealed that PAN-associated ECs highly expressed CHI3L1, SNRPD3, CLU, LAMTOR4, and AQP1, while MVP-associated ECs expressed MGP, FABP5, collagens, and modifying enzymes such as COL1A2, COL3A1, COL4A1 and COL4A2 (Fig. 5E and Table S3). Functionally, MVP endothelial cells were particularly active in cell adhesion, angiogenesis, and cytoplasmic translation pathways (Fig. 5F). To validate candidate gene expression in these regions, we conducted an in vitro module to measure mRNA expression levels in PAN and MVP regions. The results of the qPCR analysis indicated that PAN-associated genes, including CHI3L1, SNRPD3, AOP1, GUCD1, APBA2, and PTGDS, were significantly upregulated, consistent with previous analyses (Fig. S9A). Similarly, MVP-associated genes, such as FABP5, COL3A1, COL4A1, COL4A2, and SEC61G, were significantly upregulated in endothelial cells (Fig. S9B). These insights shed light on the distinct roles endothelial cells play in GBM PAN and MVP regions, highlighting the complexity and diversity of the tumor microenvironment.

Differentiation of GSCs into endothelial cells

The above results establish a link between PAN/MVP-related characterized genes and different functional states of endothelial cells in GBM. Since SRT lacks single cell resolution, we analyzed 5 GBM scRNA-seq datasets, including 2 with paired SRT. Cell types were identified **using** Seurat: T cells, microglia/macrophages, oligodendrocytes, GSCs, astrocytes, monocytes, endothelial cells, and B cells. Notably, many PAN/MVP signatures were highly or specifically expressed in endothelial cells, like AKAP12 (Fig. 6A and B). Several genes like MT1X,

MT2A, SPARC, EPAS1 and THY1 were highly expressed in both GSCs and the endothelial cells (Fig. 6A and B).

To explore intercellular communications, we visualized ligand-receptor pairs for each cell type (Fig S10). Multiple pairs involved endothelial cells, with the PTN/PTPRZ1 ligand-receptor pair a key mediator between GSCs and endothelium (Fig. 6C). Spatial heatmaps showed PTN and PTPRZ1 have similar localization (Fig. 6D). Pseudotime analysis revealed a transition trajectory from GSCs to endothelial cells (Fig. 6E and F). Correlation analysis confirmed a robust GSC-endothelial correlation (Fig. 6G). Double immunofluorescence validated this, showing colocalization of the GSC marker CD44 and the endothelial marker CD31 (Fig. 6H). This aligns with evidence that GSCs differentiate into tumor vascular endothelium [15, 16]. Together, these techniques facilitated a comprehensive analysis, providing insights into the unique gene expression profiles of GBM's perivascular and perinecrotic zones, highlighting angiogenesis, stemness, and tumorigenic signatures specific to the MVP and PAN regions.

.

Discussion

Receptor tyrosine kinases (RTKs), such as Epidermal Growth Factor Receptor (EGFR) and Platelet-Derived Growth Factor Receptor Alpha (PDGFRA), have been central molecular targets in the development of therapies for GBM [17–19]. However, limitations in drug delivery [20] imposed by the blood-brain barrier, along with complex factors in glioblastoma—such as an immunosuppressive tumor microenvironment, low immune infiltration, and high tumor heterogeneity—have significantly hindered the efficacy of immune checkpoint inhibitors in GBM [20–22]. Comprehensively characterizing histological features in a spatial context could improve GBM diagnosis and treatment. Single-cell transcriptome technology has revealed invaluable heterogeneity insights and potential therapeutic molecular targets [6, 23–25]. SRT can categorize adjacent spots into histological regions, enabling spatial heterogeneity identification between patients.
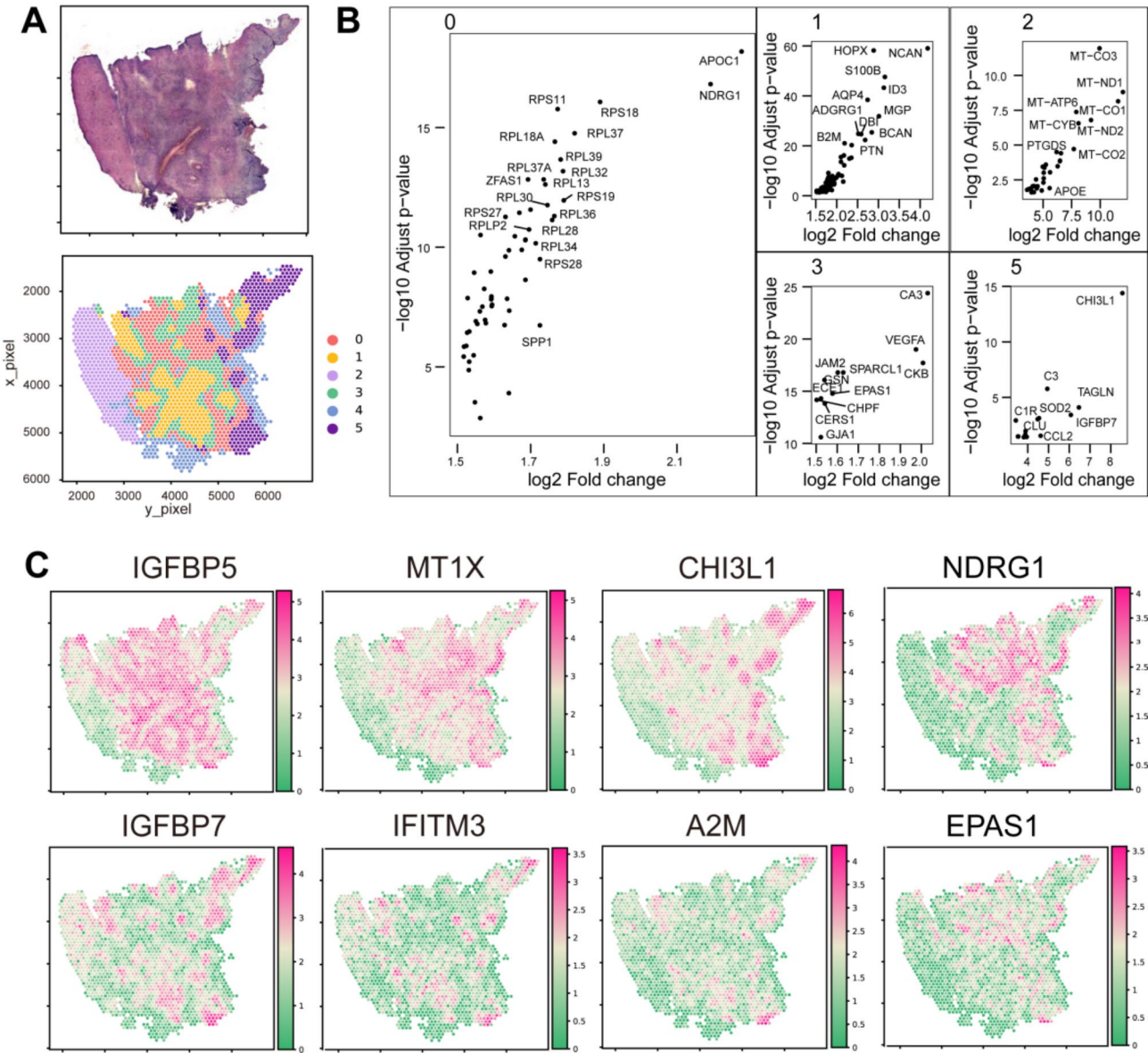
Fig. 2 The spatial localization of PAN and MVP signature genes in GBM. **A** Representative section showing different domains based on H&E-staining and spatially variable genes (SVGs). **B** Characteristically expressed genes in each domain. **C** Gene expression for eight genes on a fine grid set of spatial locations in patient UKF423

Due to differences in sampling and measurement approaches among single-cell omics, spatial transcriptomics, and bulk transcriptomics, the biological information captured by each method is not entirely consistent. Integrating and interpreting data from these three sources to extract unified biological conclusions is a significant challenge. To address this, we effectively combined the molecular features of bulk transcriptomics with single-cell clustering information to annotate cell types at individual spots in spatial transcriptomics, thereby predicting single-cell expression profiles in spatial locations. Here, we identified PAN and MVP domain-specific molecules using multi-resolution RNA sequencing, shedding light on subgrouped endothelial cells and GSC differentiation into endothelium in GBM.

Intraoperative necrosis, tumor imaging with PET (positron emission tomography) tracer fluoromisonidazole (FMISO) and histological vascular pathology highlighted
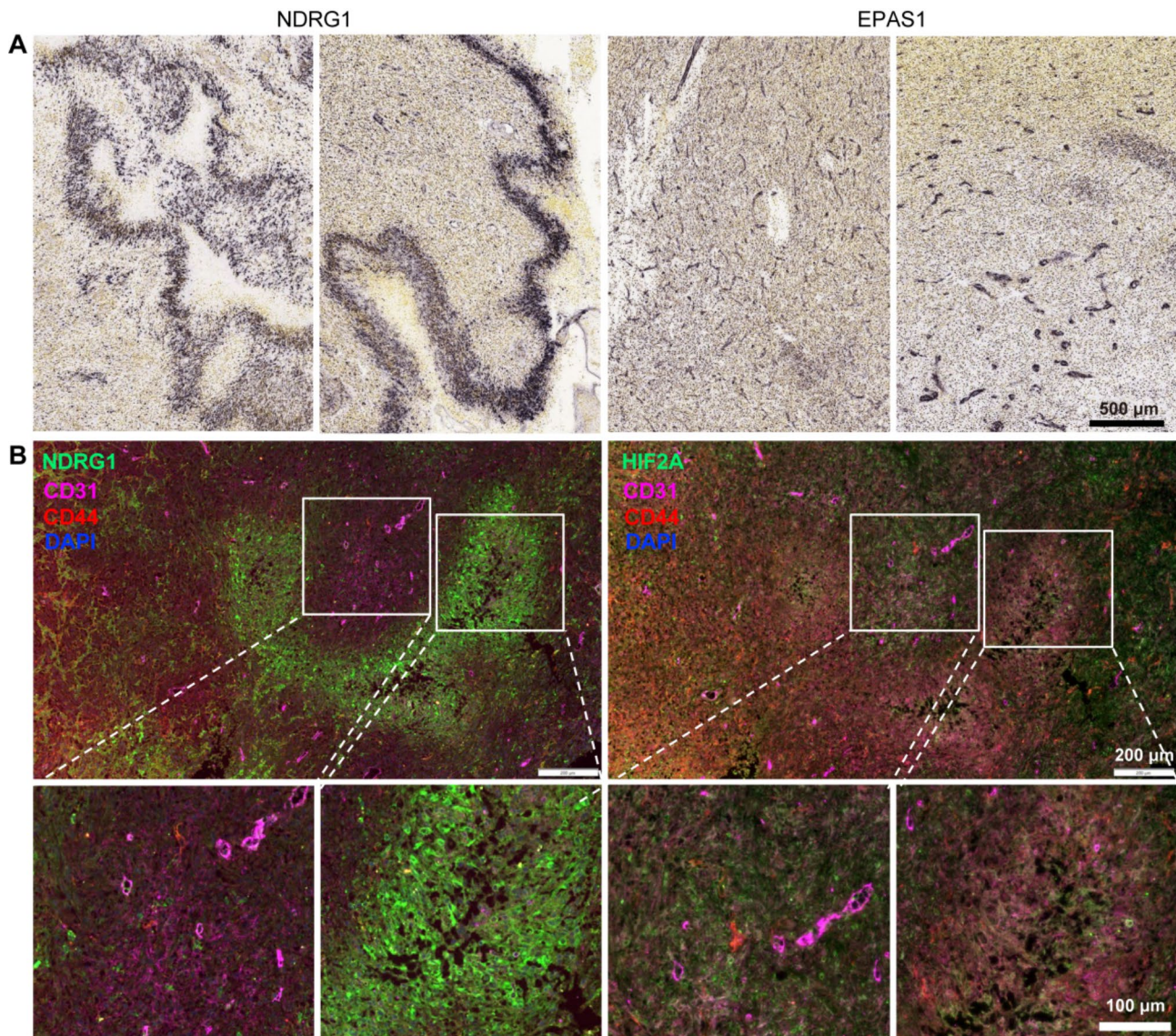
Fig. 3 Expression of NDRG1 and SPAS1 in GBM. **A** In situ hybridization (ISH) images of Ivy GAP database show PAN expression patterns of NDRG1 (left) and MVP expression patterns of EPAS1 (right) in GBM tissues. **B** Representative multiplex immunofluorescence images of NDRG1 (green), HIF2A (green) and CD31 (pink), CD44 (red) in GBM slides

hypoxia as a unique GBM pathological feature, contributing to aggressiveness [26, 27]. The hypoxia-regulated gene in GBM, N-myc-downstream regulated gene-1 (NDRG1), has been implicated in the regulating of migration, angiogenesis and drug resistance in GBM [12, 28, 29]. NDRG1 overexpression has been shown to reduce angiogenesis and tumor growth in an orthotopic glioma model [12]. Aligning with this, we found high spatial NDRG1 expression in hypoxic PAN but not MVP. We also identified other PAN signature genes like CHI3L1, encoding secreted glycoprotein YKL-40. YKL-40 modulates glioma stem cell states [11]. Recent work by Yanming Ren et al. also highlighted the enrichment of CH3CL1 in hypoxic versus invasive glioma niches [30], validating our results.

However, the biological significance of these differentially expressed genes requires further functional validation.

Angiogenesis is a critical for tumor growth and progression. Gliomas, including GBM, are highly vascularized tumors. ECs comprising blood vessels are most critical, forming capillaries that supply glioma cells. Studies using bulk or scRNA-seq have shown EC heterogeneity in GBM patients and models from different tumor sites [31, 32]. Our study introduces a new spatial dimension revealing the distinct functional states of endothelial cells in PAN and MVP regions. MVP ECs exhibited angiogenesis and high collagen expression, while PAN ECs showed hypoxia pathway activation. The MVP EC profile closely resembled the tumor core ECs reported by
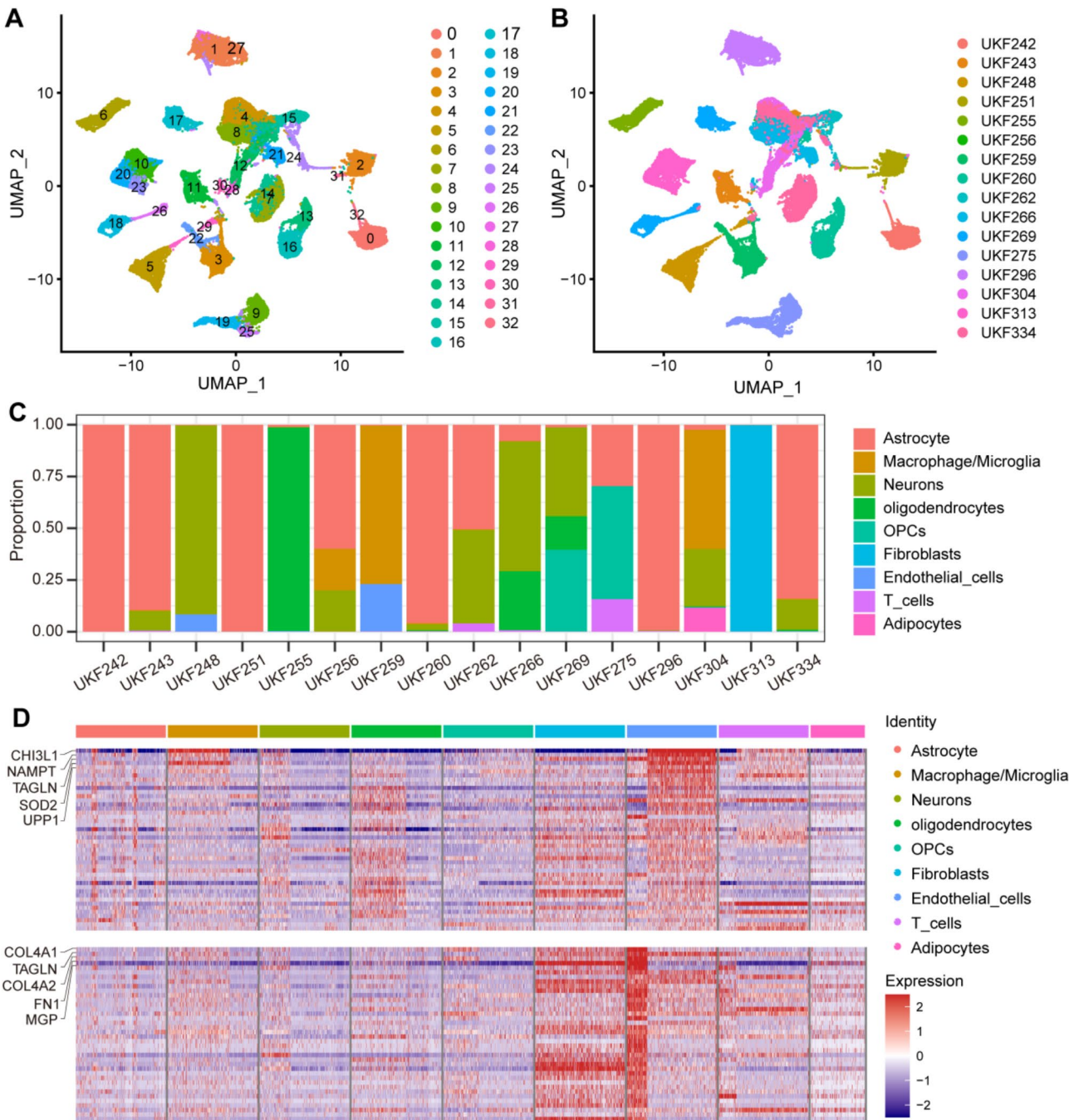
Fig. 4 UMAP visualization of human GBM SRT clusters and Cell type annotations. **A** UMAP of GBM spatial transcriptome data from 16 patients. Cells are color-coded according to the defined cluster. **B** UMAP of 16 patients. Cells are color-coded according to patient origin. **C** Percentage of each cell subset across the 16 patients. **D** Heat maps showed the expression of PAN (top) and MVP (bottom) regional characteristic genes in different cell types

Yuan Xie et al. [32]. This consistency may be due to lower EC yields from necrotic and peripheral regions in their scRNA-seq preparation (centrifugation and FACS).

Research shows GSCs reside in perivascular niches near ECs [33, 34]. Here, GSCs secrete proangiogenic VEGF, driving EC proliferation, survival, migration, and permeability [33, 35–38]. Receptor PTPRZ1 is preferentially expressed in GSCs. Inhibiting PTPRZ1 suppresses

GBM growth and prolongs survival [39, 40]. TAM-secreted PTN has been shown to stimulate PTPRZ1 on GSCs, promoting malignancy [39]. Our results suggest that PTN/PTPRZ1 and MDK/PTPRZ1 can also enable ECs-GSC communication.

It is believed GSCs can differentiate into peri-cyte-like cells supporting vessels and tumor growth [16, 41]. Recent live-cell imaging shows GSC also
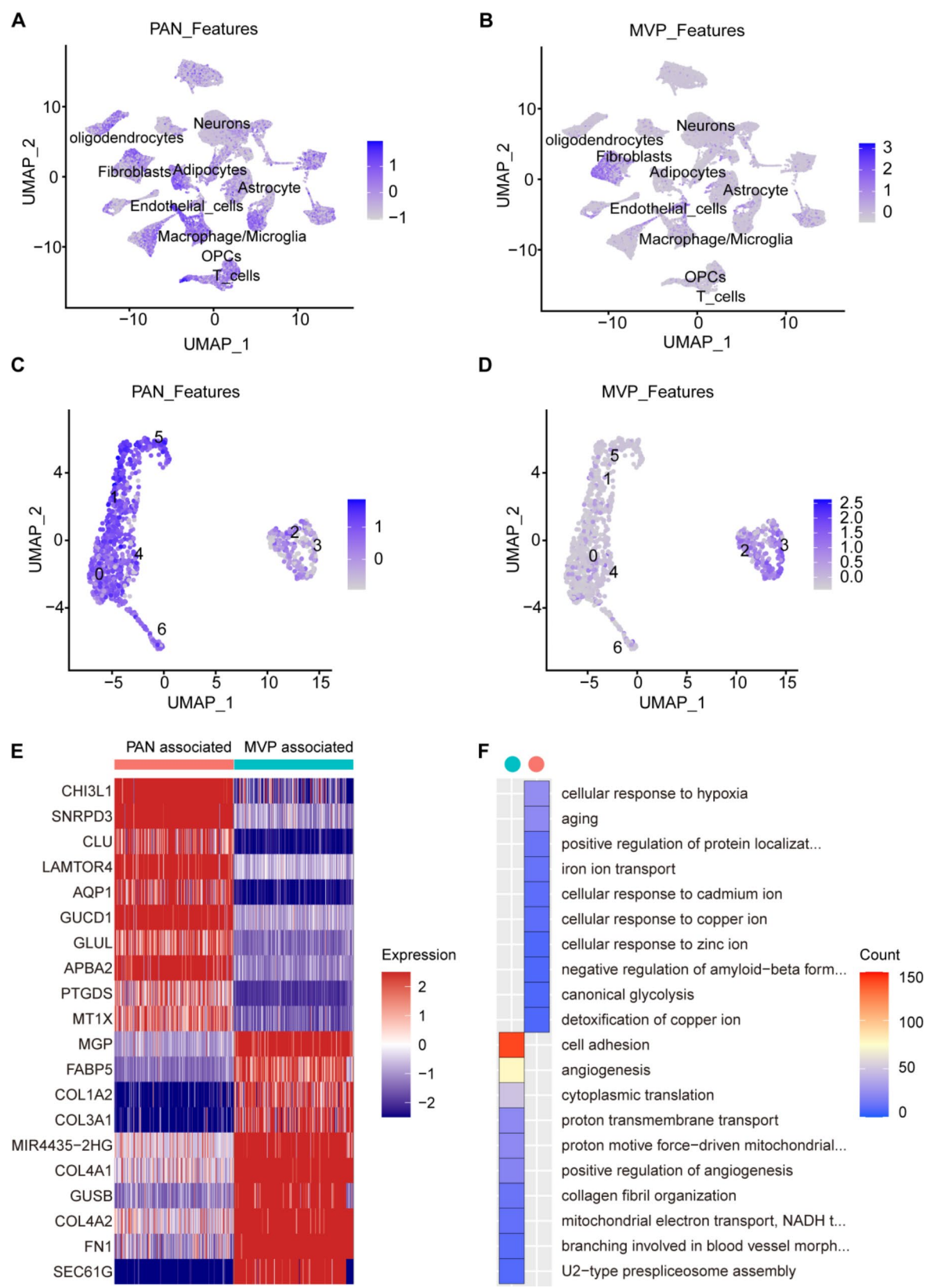
Fig. 5 Different states of endothelial cells in the PAN and MVP regions. **A**, **B** UMAP of GBM spatial transcriptome data. Composition of different kinds of cells in PAN and MVP regions was shown. **C**, **D** UMAP plot of the endothelial cells in glioma. UMAP plot colored based on the expression of PAN and MVP signatures. **E** Heatmap showing top 10 differentially expressed genes in PAN and MVP associated endothelial cells. **F** Heatmap showing top 10 enriched GO terms in different endothelial cells based on differentially expressed genes between PAN (748) and MVP (746)
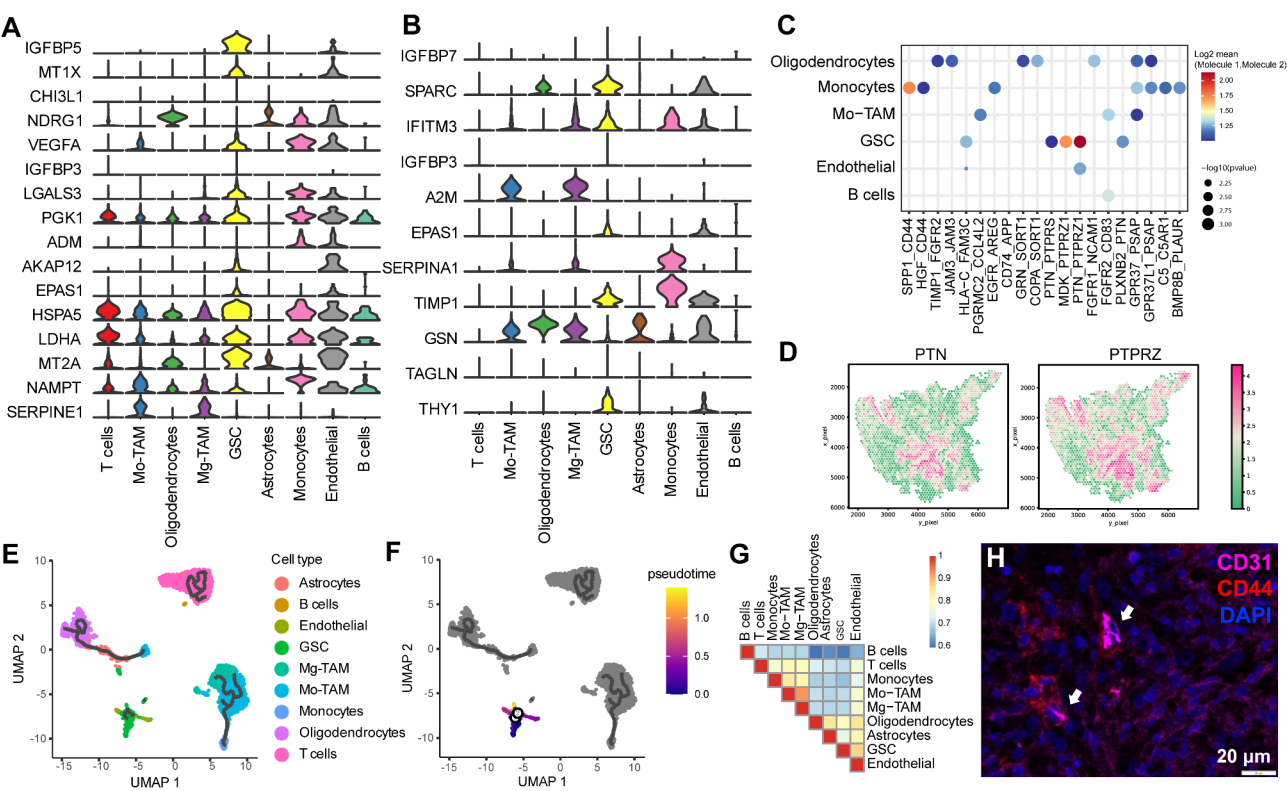
Fig. 6 Differentiation of GSCs into endothelial cells. **A**, **B** violin plots showing the normalized expression levels of signature genes across the identified cell types. **C** Dot plots showing intercellular ligand and receptor pairs between endothelial and other cell types. **D** Spatial heatmaps of PTN and PTPRZ in patient UKF423. **E** The t-SNE plot of 9 identified cell types in GBM. **F** Pseudotime analysis of single-cell RNA-seq data. **G** The correlation heatmap illustrates the relationship between pairs of cell types infiltrated in GBM. The color is scaled by the correlation value. **H** Representative multiplex immunofluorescence images of CD31 (pink) and CD44 (red) in GBM. Scale bar represents 20 μm

transdifferentiate into endothelial progenitor cells and ECs [42, 43], potentially explaining unsatisfactory anti-angiogenic glioma therapy outcomes. Our pseudotime analysis and EC-GSC marker colocalization support this.

Conclusions

This study demonstrates two distinct phenotypes of endothelial cells were enriched in the MVP and PAN regions, respectively. PAN associated ECs possess copy number variation similar to GBM cells. Single cell trajectory infers a pseudotime trajectory of glioblastoma stem cell differentiation toward ECs. Our findings provide a cellular and molecular insights into GBM progression.

Abbreviations

GBM	Glioblastoma
PAN	Pseudopalisading cells around necrosis
MVP	Microvascular proliferation
TME	Tumor microenvironment
CT	Cellular tumor
SRT	Spatially resolved transcriptomics
HBV	Hyperplastic blood vessels
PNZ	Perinecrotic zone
IT	Infiltrating tumor
LE	Leading edge

Supplementary Information

The online version contains supplementary material available at https://doi.org/10.1186/s12967-025-06185-z.

Supplementary Material 1

Supplementary Material 2

Supplementary Material 3

Supplementary Material 4

Supplementary Material 5

Data availability
The Spatially resolved transcriptomics (SRT) datasets were obtained from https://doi.org/10.5 061/dryad.h70rxwdmj. The smart-seq2 glioblastoma scRNA-seq dataset (*n* = 28, GSE131928) was downloaded from the GEO database. The Cancer Genome Atlas (TCGA) GBM dataset (*n* = 155), including RNA-sequencing, clinical, was obtained from the UCSC Xena browser (https://xenabrowser.net/). No specific code was generated for analysis of these data. If you have any questions regarding the code, feel free to contact the corresponding author of the article at any time.

Declarations

Ethics approval and consent to participate
All glioma samples were collected with signed informed consent according to the internal review and ethics boards of Wuhan Union Hospital. The procedure was approved by the ethics boards of Wuhan Union Hospital.

Consent for publication
Not applicable.

Competing interests
The authors declare no competing interests.

Author details
[1]School of Biomedical Engineering (Suzhou), Division of Life Sciences and Medicine, University of Science and Technology of China, Hefei 230026, China
[2]Department of Biomaterials and Stem Cells, Suzhou Institute of Biomedical Engineering and Technology, Chinese Academy of Sciences, Keling Road No.88, Suzhou 215163, China
[3]Department of Chemistry, College of Sciences, Shanghai University, Shanghai 200444, China
[4]Department of Neurosurgery, Suzhou Hospital, Affiliated Hospital of Medical School, Nanjing University, Lijiang Road No. 1, Suzhou 215153, China
[5]Institute of Biomedical & Genetic Engineering, 24-Mauve Area G-9/1, Islamabad 44000, Pakistan
[6]Institute of Pharmaceutical Sciences, Khyber Medical University, F1 Phase-6 Rd, Phase 5 Hayatabad, Peshawar, Khyber Pakhtunkhwa 25100, Pakistan
[7]Institute of Clinical Medicine Research, Suzhou Hospital, Affiliated Hospital of Medical School, Nanjing University, Lijiang Road No. 1, Suzhou 215153, China

References
1. Wen PY, Packer RJ. The 2021 WHO classification of tumors of the Central Nervous System: clinical implications. Neurooncology. 2021;23(8):1215–7.
2. Horbinski C, et al. Clinical implications of the 2021 edition of the WHO classification of central nervous system tumours. Nat Reviews Neurol. 2022;18(9):515–29.
3. Barajas RF Jr., et al. Glioblastoma multiforme regional genetic and cellular expression patterns: influence on anatomic and physiologic MR imaging. Radiology. 2010;254(2):564–76.
4. McBain C, et al. Treatment options for progression or recurrence of glioblastoma: a network meta-analysis. Cochrane Database Syst Rev. 2021;5(1):CD013579.
5. Bhaduri A, et al. Outer radial glia-like Cancer stem cells contribute to heterogeneity of Glioblastoma. Cell Stem Cell. 2020;26(1):48–e636.
6. Neftel C, et al. An Integrative Model of Cellular States, plasticity, and Genetics for Glioblastoma. Cell. 2019;178(4):835–e84921.
7. Pan KF, et al. Direct interaction of beta-catenin with nuclear ESM1 supports stemness of metastatic prostate cancer. EMBO J. 2021;40(4):e105450.
8. Wang J, et al. CRIP1 suppresses BBOX1-mediated carnitine metabolism to promote stemness in hepatocellular carcinoma. EMBO J. 2022;41(15):e110218.
9. Lin W, et al. IGFBP5 is an ROR1 ligand promoting glioblastoma invasion via ROR1/HER2-CREB signaling axis. Nat Commun. 2023;14(1):1578.
10. Dixit D, et al. The RNA m6A reader YTHDF2 maintains Oncogene expression and is a targetable dependency in Glioblastoma Stem cells. Cancer Discov. 2021;11(2):480–99.
11. Guetta-Terrier C, et al. Chi3l1 is a modulator of Glioma Stem Cell States and a therapeutic target in Glioblastoma. Cancer Res. 2023;83(12):1984–99.
12. Broggini T, et al. NDRG1 overexpressing gliomas are characterized by reduced tumor vascularization and resistance to antiangiogenic treatment. Cancer Lett. 2016;380(2):568–76.
13. Si M, Lang J. The roles of metallothioneins in carcinogenesis. J Hematol Oncol. 2018;11(1):107.
14. Lin S, et al. Transcription factor myeloid zinc-finger 1 suppresses human gastric carcinogenesis by interacting with metallothionein 2A. Clin Cancer Res. 2019;25(3):1050–62.
15. Ricci-Vitiani L, et al. Tumour vascularization via endothelial differentiation of glioblastoma stem-like cells. Nature. 2010;468(7325):824–8.
16. Hu B, et al. Epigenetic activation of WNT5A drives glioblastoma stem cell differentiation and invasive growth. Cell. 2016;167(5):1281–e129518.
17. Marin BM, et al. Heterogeneous delivery across the blood-brain barrier limits the efficacy of an EGFR-targeting antibody drug conjugate in glioblastoma. Neuro Oncol. 2021;23(12):2042–53.
18. Dunn GP, et al. Emerging insights into the molecular and cellular basis of glioblastoma. Genes Dev. 2012;26(8):756–84.
19. Verhaak RG, et al. Integrated genomic analysis identifies clinically relevant subtypes of glioblastoma characterized by abnormalities in PDGFRA, IDH1, EGFR, and NF1. Cancer Cell. 2010;17(1):98–110.
20. Samantasinghar A, et al. A comprehensive review of key factors affecting the efficacy of antibody drug conjugate. Biomed Pharmacother. 2023;161:114408.
21. Wang Q, et al. Tumor evolution of Glioma-Intrinsic Gene Expression Subtypes Associates with immunological changes in the Microenvironment. Cancer Cell. 2018;33(1):152.
22. Ahmed F et al. Network-based drug repurposing identifies small molecule drugs as immune checkpoint inhibitors for endometrial cancer. Mol Divers, 2024.
23. Darmanis S, et al. Single-cell RNA-Seq analysis of infiltrating neoplastic cells at the Migrating Front of Human Glioblastoma. Cell Rep. 2017;21(5):1399–410.
24. Richards LM, et al. Gradient of Developmental and Injury Response transcriptional states defines functional vulnerabilities underpinning glioblastoma heterogeneity. Nat Cancer. 2021;2(2):157–73.
25. Tirosh I, et al. Single-cell RNA-seq supports a developmental hierarchy in human oligodendroglioma. Nature. 2016;539(7628):309–13.
26. Gerstner ER, et al. ACRIN 6684: Assessment of Tumor Hypoxia in newly diagnosed Glioblastoma using 18F-FMISO PET and MRI. Clin Cancer Res. 2016;22(20):5079–86.
27. Yamamoto Y, et al. Hypoxia assessed by 18F-fluoromisonidazole positron emission tomography in newly diagnosed gliomas. Nucl Med Commun. 2012;33(6):621–5.
28. Zhang X et al. *N-myc Downstream-Regulated Gene 1 (NDRG1) Regulates Vascular Endothelial Growth Factor A (VEGFA) and Malignancies in Glioblastoma Multiforme (GBM)*. Biomed Res Int, 2022. 2022: p. 3233004.
29. Weiler M, et al. mTOR target NDRG1 confers MGMT-dependent resistance to alkylating chemotherapy. Proc Natl Acad Sci U S A. 2014;111(1):409–14.
30. Ren Y, et al. Spatial transcriptomics reveals niche-specific enrichment and vulnerabilities of radial glial stem-like cells in malignant gliomas. Nat Commun. 2023;14(1):1028.
31. Carlson JC, et al. Identification of diverse tumor endothelial cell populations in malignant glioma. Neuro Oncol. 2021;23(6):932–44.
32. Xie Y et al. Key molecular alterations in endothelial cells in human glioblastoma uncovered through single-cell RNA sequencing. JCI Insight, 2021. 6(15).
33. Prager BC, et al. Glioblastoma Stem Cells: driving resilience through Chaos. Trends Cancer. 2020;6(3):223–35.
34. Kumar S, et al. Identification of vascular cues contributing to cancer cell stemness and function. Angiogenesis. 2022;25(3):355–71.
35. Jain RK, et al. Angiogenesis in brain tumours. Nat Rev Neurosci. 2007;8(8):610–22.

36. Li D, et al. Glioma-associated human endothelial cell-derived extracellular vesicles specifically promote the tumourigenicity of glioma stem cells via CD9. Oncogene. 2019;38(43):6898–912.

37. Sharma A, Shiras A. Cancer stem cell-vascular endothelial cell interactions in glioblastoma. Biochem Biophys Res Commun. 2016;473(3):688–92.

38. Adjei-Sowah EA, et al. Investigating the Interactions of Glioma Stem Cells in the Perivascular Niche at single-cell resolution using a microfluidic Tumor Microenvironment Model. Adv Sci (Weinh). 2022;9(21):e2201436.

39. Shi Y, et al. Tumour-associated macrophages secrete pleiotrophin to promote PTPRZ1 signalling in glioblastoma stem cells for tumour growth. Nat Commun. 2017;8:15080.

40. Yang M, et al. PTN-PTPRZ1 signaling axis blocking mediates tumor microenvironment remodeling for enhanced glioblastoma treatment. J Control Release. 2023;353:63–76.

41. Cheng L, et al. Glioblastoma stem cells generate vascular pericytes to support vessel function and tumor growth. Cell. 2013;153(1):139–52.

42. Han X, et al. P4HA1 regulates CD31 via COL6A1 in the transition of Glioblastoma Stem-Like cells to Tumor Endothelioid cells. Front Oncol. 2022;12:836511.

43. Mei X, et al. Glioblastoma stem cell differentiation into endothelial cells evidenced through live-cell imaging. Neuro Oncol. 2017;19(8):1109–18.

Publisher's note